# Single crystals of metal-organic framework Ulm-4 grown selectively on a micro-structured plasma polymer coating

**Andreas Schaller, Aladin Baldur Bernd Ullrich, Dirk Volkmer**

**Angaben zur Veröffentlichung / Publication details:**

Schaller, Andreas, Aladin Baldur Bernd Ullrich, and Dirk Volkmer. 2019. "Single crystals of metal-organic framework Ulm-4 grown selectively on a micro-structured plasma polymer coating." *Thin Solid Films* 684: 36–41. https://doi.org/10.1016/j.tsf.2019.05.050.

# Single crystals of Metal-Organic Framework Ulm-4 grown selectively on a micro-structured plasma polymer coating

Andreas Schaller[a], Aladin Ullrich[b], Dirk Volkmer[a,*]

[a] University of Augsburg, Chair of Solid State & Materials Chemistry, Universitaetsstrasse 1, 86156 Augsburg, Germany
[b] University of Augsburg, Chair of Experimental Physics II, Universitaetsstrasse 1, 86156 Augsburg, Germany

## 1. Introduction

Applying a cold or non-thermal plasma to a solid material is a common method to modify its surface, e.g. by eliminating unwanted residues or by oxidizing the topmost layers of the material [1–3]. Besides these ablation or etching processes a non-thermal plasma can also be employed to deposit thin, polymer-like coatings on variable substrates from monomers which are not accessible for standard polymerization reactions. This technique is often referred to as plasma polymerization or more specifically plasma enhanced chemical vapor deposition [4]. By tuning process parameters such as power input or monomer composition the resulting coatings can be adjusted to show either higher cross-linking, and thus high chemical stability, or retention of the monomer structure [5]. However, it is possible to generate films that provide high retention of the functional groups and satisfying stability [6]. The chemical and physical properties – like surface energy and film thickness – can be altered by varying the chosen monomer(s) and the polymerization conditions during the deposition process (i.e. pressure, power input, and duration) [4,7]. The combination of high chemical stability and adjustable surface chemistry offers the possibility to generate templates for the selective growth of crystals of demanding functional materials such as metal-organic frameworks (MOFs). MOFs are porous materials which have very large internal surface areas of up to 6000 $m^2/g$ [8]. Several reviews report the application potential of MOFs for gas separation [9], gas storage [10], and heterogeneous catalysis [11]. Furthermore, MOFs are suitable for chemical sensing devices for gases or vaporous molecules [12]. These sensors often require that the MOF crystals are mounted as a thin film on some sort of substrate to form a chemically responsive layer. The on-substrate-growth of several MOFs like Metal-Organic Framework-5 [13], Hong Kong University of Science and Technology-1 (HKUST-1) [14,15], or Zeolitic Imidazolate Framework-8 [16] among others [17] has been shown.

The signal transduction from the loaded MOF to an evaluable readout is an important point in designing a working sensing device. Several methods are suggested for the realization of such a sensor [18,19]. Allendorf et al. reported the first functional sensing device featuring HKUST-1 grown on a self-assembled monolayer (SAM) [20]. Similar approaches with SAM substrates were pursued by several other groups [21–24]. Furthermore, the shape and the orientation of the crystals grown on substrates can be influenced to demonstrate only a specific form of appearance [25–27]. A different take on was first published by Dimitrakakis reporting a patterned plasma polymer coating employed as a substrate to produce a likewise patterned layer of MOF crystals [28]. The variety of accessible monomers compared with the enhanced chemical stability of the resulting plasma coatings offers the feasibility of engineering robust micro-patterned MOF thin films used in MOF sensors [29] or MOF microelectronic devices [30]. Our group showed recently, that MOFs which require harsh synthesis conditions incompatible with SAMs [31,32] can be grown on plasma coatings [33]. In this work we present an approach of selective MOF crystal growth on the hydrophilic domains of a patterned multilayer plasma polymer coating composed of hydrophilic and hydrophobic regions. The latter consists of plasma-polymerized trifluoromethane, which forms a coating with similar surface properties like polytetrafluoroethylene (PTFE).

* Corresponding author.
*E-mail address:* dirk.volkmer@physik.uni-augsburg.de (D. Volkmer).

## 2. Experimental

### 2.1. Plasma etching and deposition of plasma coatings

All plasma processes were carried out employing a FEMTO plasma system (Diener electronic, Germany) previously described in detail [34]. The device features two power generators, the first working at a frequency of 13.56 MHz while the other one is operated at 40 kHz; both offer pulsed and continuous modes at a maximum power output of 300 W. The pressure of the volatile monomers introduced into the reaction chamber ranges from 10 to 80 Pa. The volume of the reaction chamber is approximately 6 $dm^3$. Two types of substrates were used for our experiments, either silicon substrates or glass substrates. Which type of substrate was used is described in the corresponding section. Before applying the plasma coatings, all substrates were etched using an oxygen plasma for 30 min in order to remove unwanted residues on the surface and to provide a homogeneous silica surface. After this etching process three subsequent layers of plasma polymer coatings were deposited. All deposition processes were carried out with monomers which are normally not available for polymerization reactions. The first layer serves as a coupling agent between the silica substrate and the subsequent organic plasma coating and is composed of plasma-polymerized hexamethyldisiloxane (ppHMDSO). The next layer consists of plasma-polymerized propionic acid (ppPA), which provides hydrophilic moieties. The final coating of plasma-polymerized trifluoromethane (ppTFM) resembles a PTFE-like hydrophobic coating. The conditions for the etching and deposition steps are shown in Table 1. For the deposition of the ppTFM layer argon was employed as a carrier gas with a flow rate of 32 $cm^3$/min.

### 2.2. Micro-structuring of the plasma coatings

The multilayer plasma polymer coatings were then micro-structured via irradiation with ultra violet (UV) light through a patterned quartz mask in a custom-made lithography system [35]. All components of the system were obtained from Hamamatsu Photonics K.K. (Japan). The light source consists of a 250 nm enhanced 200 W mercury-xenon lamp (LC 8 L9588-02A) with a wavelength range from 240 to 400 nm. The measured optical power which reaches the sample surface after its way through the optical setup with a synthetic silica light guide (A10015–50-0110, length = 1 m, diameter = 5 mm) and a beam distributor (E5147–06) was 94 mW/$cm^2$. The scan range of the power meter reaches from 250 to 2200 nm. The measured power was integrated within that range. The distance between the lower lens of the beam distributor and the sample surface was 16 cm. The quartz masks have a pattern of transparent circles of 20 µm diameter. The UV-lithographic process was carried out for 90 min at ambient conditions. Afterwards, the coatings were rinsed twice with deionized water and then dried with compressed air. UV lithographic etching of the samples resulted in periodic, circular cavities corresponding to the pattern of the mask. The step height of the cavities was adjusted to have its bottom in the hydrophilic ppPA layer by choosing the duration of the irradiation in an appropriate way. The schematic architecture of the final patterned coating consisting of the three consecutive plasma layers is depicted in Fig. 1.

**Table 1**
Conditions used for deposition and etching processes.

| Gas/monomer | O2 | ppHMDSO | ppPa | ppTFM |
|---|---|---|---|---|
| Power [W] | 300 | 150 | 150 | 150 |
| Frequency | 13.56 MHz | 40 kHz | 40 kHz | 40 kHz |
| Mode | continuous | pulsed | pulsed | pulsed |
| Duration [min] | 30 | 1 | 90 | 5 |
| Pressure [Pa] | 30 | 50 | 55 | 85 |

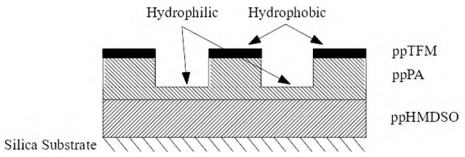


**Fig. 1.** Schematic build-up of the structured multilayer coating. The depiction is for better visibility not true to scale.

**Table 2**
Values of contact angle measurements before and after irradiation of a sample and of a PTFE sample.

| | Before UV | After UV | PTFE comparison |
|---|---|---|---|
| CA ($H_2O$) [°] | 115 | 13 | 120 |
| CA ($CH_2I_2$) [°] | 75 | 71 | 75 |
| SE [mN/m] | 20 | 71 | 20 |

### 2.3. MOF synthesis

Glass substrates with micro-structured plasma coatings were immersed in a typical mother liquor used for solvothermal synthesis of Metal-Organic Framework Ulm-4 (MFU-4) crystals [36]. In a closed reaction vessel 1.0 mg (6.25 µmol) of the linker $H_2$-bbta (=1H, 5H-benzo(1,2-d:4,5-d´)bistriazol) was dissolved in 2 mL dimethylformamide (p.a.). After the organic linker had completely dissolved, 3.4 mg (0.025 mmol) $ZnCl_2$ were added. A glass substrate coated with a micro-patterned plasma polymer film was directly placed in the reaction vessel on a small PTFE ring, with the coating facing downward. The closed reaction vessel was heated at 90 °C for 60 min. After cooling the reaction medium down to room temperature, the glass substrate was removed from the vessel and rinsed twice with dimethylformamide (p.a.) and twice with ethanol (p.a.).

### 2.4. Surface characterization of plasma polymer coatings

The characterization of the surface properties of the plasma polymer coatings was conducted with contact angle (CA) respectively surface energy (SE) measurements. The measurements were carried out on plasma polymer model samples, which were either irradiated without a quartz mask, to generate a sample with a completely hydrophilic surface, or not irradiated at all, to form a thoroughly hydrophobic model sample. The CA measurements were conducted at ambient conditions using a Kruess DSA25E setup (Germany) and demineralized water or diiodomethane. For all measurements the droplet volume was 2 µL.

The characterization of the surface chemistry of the plasma polymer substrates was further investigated with X-ray photoelectron spectroscopy (XPS). The plasma coating samples for the XPS measurements were prepared in the same way as the model samples for the CA measurements, except that silicon wafer substrates were used instead of glass ones because the substrate has to be conductive. The plasma etching and all deposition steps were carried out analogous to the method with glass substrates. Also, for XPS measurements the UV irradiation was performed on the whole coating surface without employing a mask. The XPS device (Omicron, Germany) features a monochromatic Mg anode (XM 1000 Mk II, 1486.7 eV) and a hemispherical analyzer (EA 125).

Auger spectroscopy and Auger mapping scans were performed employing a NANO-SAM (Omicron, Germany). Instead of glass, silicon was chosen as the substrate material and etching, deposition steps, as well as UV-lithography were carried out in the same manner as with glass substrates. The background-corrected map was generated by using the formula $I = (p\text{-}b)/(p \pm b)$, where $I$ is the corrected intensity, $p$ the fluorine peak intensity, and $b$ the background intensity.

Topographical studies were done with a 5500 scanning probe

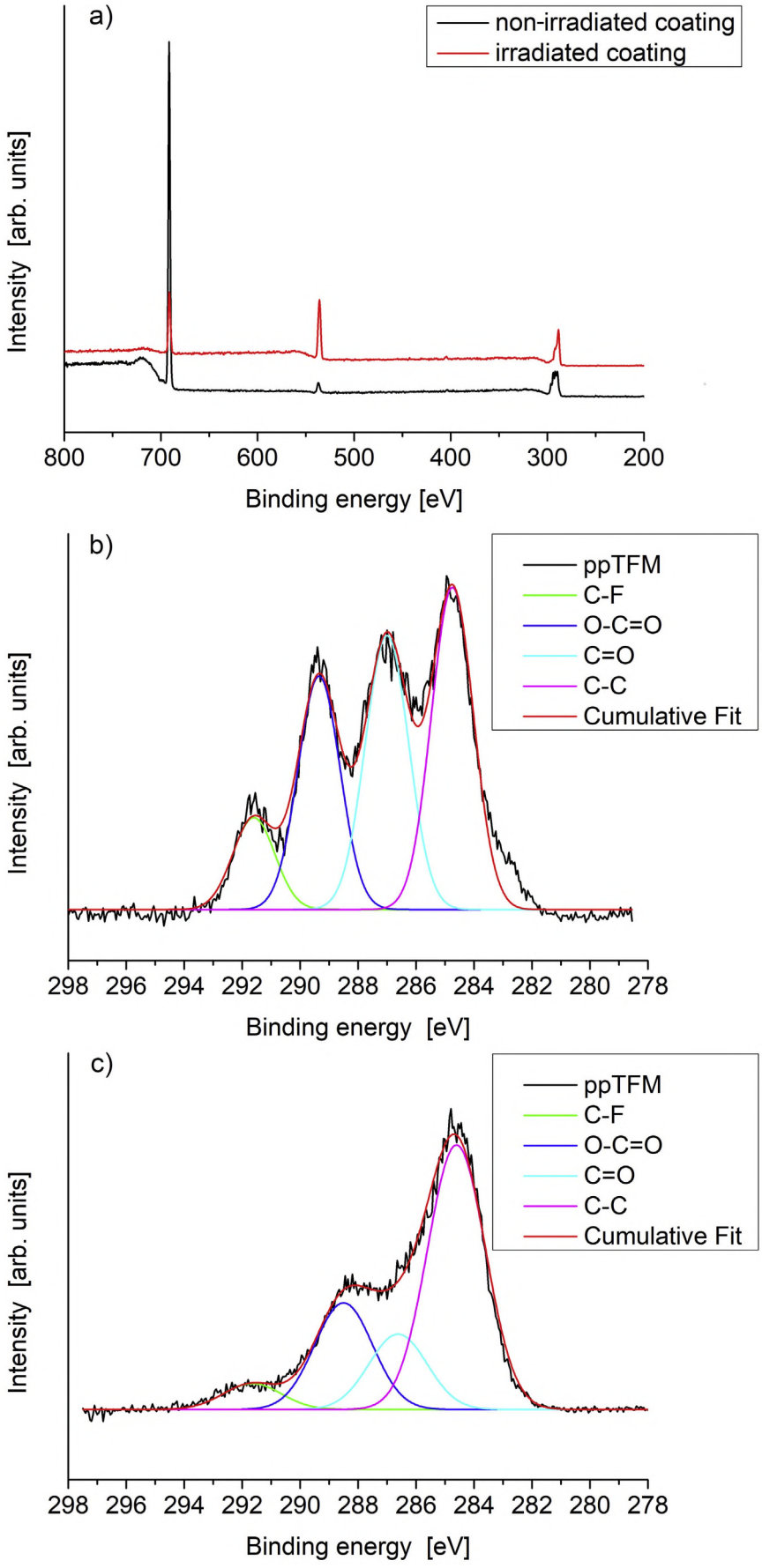


*(caption on next page)*

**Fig. 2.** (a) XPS measurements of irradiated (black) and non-irradiated (red) multilayer plasma polymer coating. XPS C 1 s region of a non-irradiated (b) and irradiated (c) multilayer plasma polymer coating (black) with four fit functions at 292 eV, 290 eV, 287 eV and 284.5 eV and the resulting cumulative fit (red). (For interpretation of the references to color in this figure legend, the reader is referred to the web version of this article.)

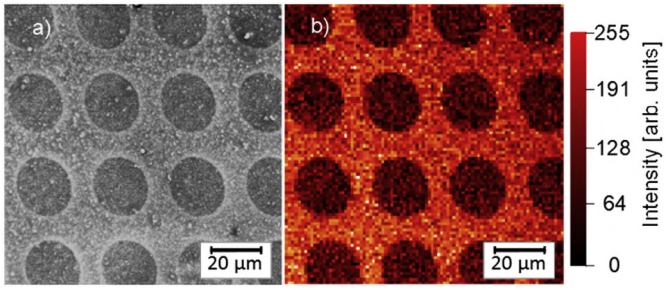


**Fig. 3.** (a) SEM micrograph and (b) fluorine Auger mapping of a micro-structured plasma polymer model sample.

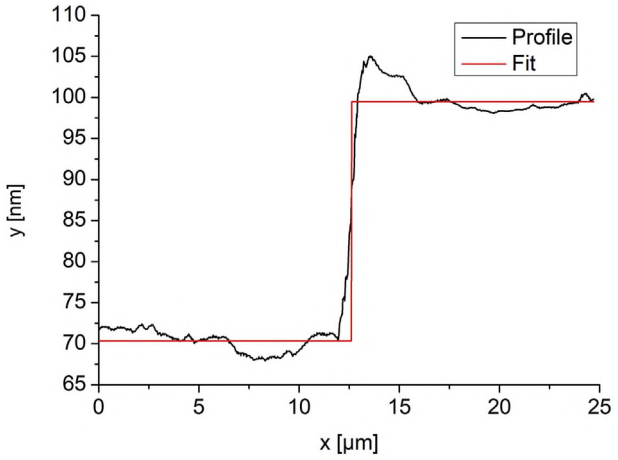


**Fig. 4.** Topographical AFM scan of a micro-structured plasma polymer coating.

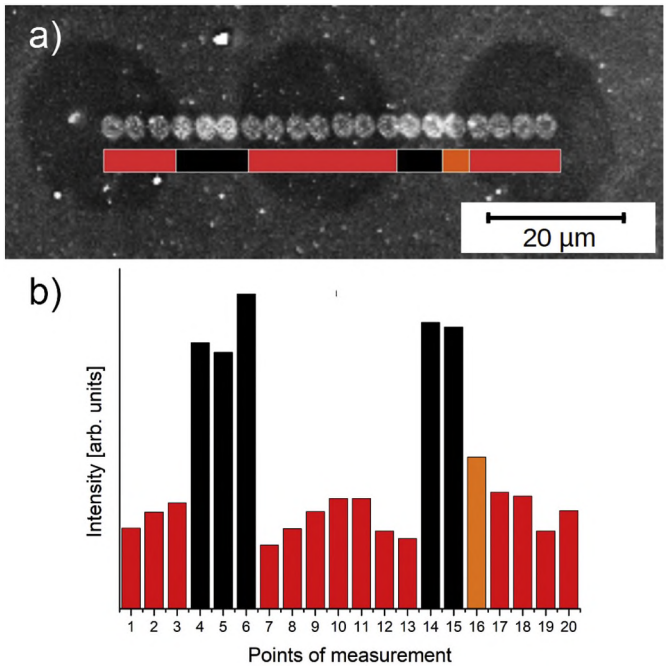


**Fig. 5.** (a) SEM micrograph of the sample area from which the Auger linescans shown were obtained. The electron beam was defocused to prevent damaging the sample. (b) Baseline-corrected bar graph of the XPS intensities at 660 eV for each measuring point of the linescan.

atomic force microscope (AFM), Agilent Technologies (USA) featuring a MAC III controller and a closed loop multipurpose scanner. All measurements were conducted in alternating contact mode with an OMCL-AC160TS cantilever, Olympus K.K. (Japan).

### 2.5. MOF characterization

Scanning electron microscopy (SEM) micrographs were carried out with an XL 30 ESEM FEG, FEI (USA) in environmental mode with back scattered electrons detector. The accelerating voltage was 10 kV, the probe current approximately 290 µA and the working distance 4 mm.

X-ray powder diffraction (XRD) was conducted with a Seifert XRD 3003 TT (Germany). The device has a Meteor 1D detector working at 40 kV and 40 mA a $CuK_{\alpha}$ x-ray source with $\lambda = 0.154247$ nm.

## 3. Results and discussion

The CAs of demineralized water and diiodomethane on the non-irradiated sample match very closely the respective CAs of a commercially available PTFE-tape comparison sample. But after irradiation the $CA_{H2O}$ decreases from 115° to 13° and the SE increases from 20 mN/m to 71 mN/m (see Table 2), which indicates that there is a drastic change of the surface chemistry of the plasma polymer coating during UV irradiation.

The resulting XPS data indicate that the amount of fluorine decreases by more than 70% and the amount of oxygen increases by more than 85%. Whereas the amount of carbon only changes by about 17%. Fig. 2a illustrates the change of the relative occurrence of fluorine, oxygen and carbon on the surface of the two model coatings. Detailed XPS analysis of the C 1 s signal of the non-irradiated substrate showed that there are four distinctive binding energies corresponding to four different types of chemical bonds (see Fig. 2b). After irradiation, the signal of the C—F and the C—O bond is drastically reduced corresponding to the removal of the topmost layer of the coating and the uncovering of the ppPA layer (see Fig. 2c.)

In order to demonstrate the spatial boundaries of the chemical changes introduced to the fluorinated plasma polymer film, Auger spectroscopy was applied to patterned model samples. Fig. 3a shows a SEM micrograph of plasma coating with a circular pattern. The darker circles correspond to the irradiated areas which are lower in height than the non-irradiated (brighter) areas. In Fig. 3b the same area is shown in a false color depiction. The brightness corresponds directly to the detected amount of fluorine. According to atomic force microscopy the step height is approximately 25 nm (see Fig. 4).

An Auger linescan was performed over the different domains of the structured sample to emphasize the sharp spatial distinction between the hydrophilic and hydrophobic domains. Fig. 5a illustrates the progression of the linescan on the surface of the sample. The scan direction is from left to right. Each of the 20 small circles corresponds to an intensity of the bar graph in Fig. 5 b. The color of the bar graphs also corresponds to the color of the bar directly below the measurement points of Fig. 5 a.

Fig. 5b shows the baseline corrected Auger intensities at 660 eV for the 20 measurement points of the linescan. The first three bars (red) show a low or no intensity due to the absence of fluorine. The next three bars have a significantly higher intensity, which then again is reduced for the next six bars. These first 12 bars show the sharp distinction between the non-fluorinated gaps and the fluorine containing bridges of the sample. The 16th spectrum was collected from a spot which tangents both domains therefore the bar has a medium intensity.

SEM micrographs of the samples after immersion into the MOF

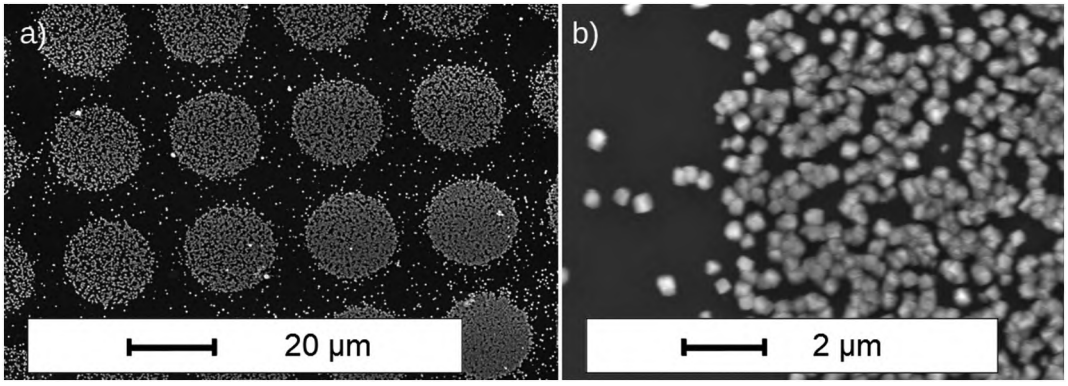


**Fig. 6.** SEM micrographs of MFU-4 crystals on a micro-structured sample at a magnification of 1000× (a) and 10,000× (b).

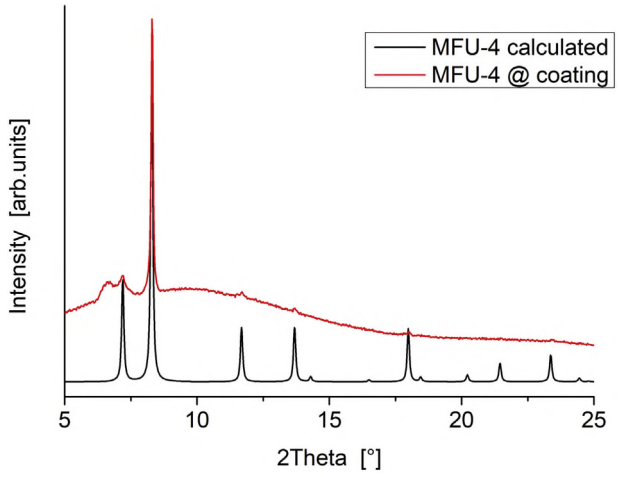


**Fig. 7.** Comparison of a measured XRD pattern of MFU-4 grown on an UV-irradiated plasma-coated substrate (red) and of a simulated powder pattern (black). (For interpretation of the references to color in this figure legend, the reader is referred to the web version of this article.)

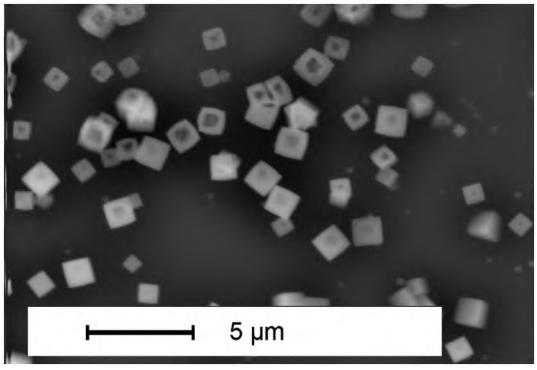


**Fig. 8.** SEM micrograph of cubic MFU-4 crystals. To improve the visibility of the crystals, the reaction time was increased to 15 h.

mother liquor show spatially defined areas of MFU-4 crystal growth preferentially in the hydrophilic areas of the structured sample (see Fig. 6a – b). The size distribution of the cubic MFU-4 crystals is quite narrow with each crystal edge being about 250 nm long. X-ray diffraction analysis of the crystals grown on the substrate confirmed the formation of MFU-4 crystals. Fig. 7 depicts the comparison of a measured powder pattern (red line) with a simulated powder pattern (black line). The two patterns show an accordance of six reflections at 2Theta = 7.0°, 8.2°, 11.6°, 13.6°, 17.9° and 23.3°. The cubic shape of the crystals (see Fig. 8) points towards the formation of single crystals of MFU-4. Unfortunately, neither XRD analysis nor SEM micrographs suggest a specific orientation of the crystals grown on the hydrophilic domains.

## 4. Conclusions

In summary, we demonstrate the feasibility of spatially directed growth of crystals of the functional material MFU-4 on an easy to produce, chemically robust, multilayer plasma polymer coating with an alternating hydrophilic/hydrophobic micro-structured pattern. Controlling the spatial allocation of a metal-organic framework is an attractive goal in the development of miniaturized, more efficient gas sensing devices.

## Acknowledgements

The authors would like to thank E. Lachner (Chair of Experimental Physics II, University of Augsburg) for performing the XPS measurements. We also want to thank P. del Forno for her proofreading of this article. Dirk Volkmer is grateful for financial support by DFG priority program 1928: Coordination Networks: Building Blocks for Functional Systems (Germany).

## References

[1] R. d'Agostino, Plasma Deposition, Treatment, and Etching of Polymers, Academic Press Inc, San Diego, 1990.
[2] D.M. Manos, D.L. Flamm, Plasma Etching an Introduction, Academic Press, Inc, San Diego, 1989.
[3] M. Sugawara, Plasma Etching: Fundamentals and Applications, Oxford University Press, Oxford, 1998.
[4] H. Yasuda, Glow discharge polymerization, J. Polym. Sci. 16 (1981) 199–293.
[5] P. Rupper, M. Vandenbossche, L. Bernard, D. Hegemann, M. Heuberger, Composition and stability of plasma polymer films exhibiting vertical chemical gradients, Langmuir 33 (2017) 2340–2352.
[6] B. Finke, K. Schröder, A. Ohl, Structure retention and water stability of microwave plasma polymerized films from Allylamin and acrylic acid, Plasma Process. Polym. 6 (2009) 70–74.
[7] H. Yasuda, T. Hsu, Some aspects of plasma polymerization investigated by pulsed R.F. discharge, J. Polym. Sci. A1 15 (1977) 81–97.
[8] H.-C. Zhou, J.R. Long, O.M. Yaghi, Introduction to metal-organic frameworks, Chem. Rev. 112 (2012) 673–674.
[9] J.-R. Li, J. Sculley, H.-C. Zhou, Metal-organic frameworks for separations, Chem. Rev. 112 (2012) 869–932.
[10] R.E. Morris, P.S. Wheatley, Gas storage in Nanoporous materials, Angew. Chem. Int. Ed. 47 (2008) 4966–4981.
[11] L. Ma, C. Abney, W. Lin, Enantioselective catalysis with Homochiral metal-organic frameworks, Chem. Soc. Rev. 38 (2009) 1248–1256.
[12] L.E. Kreno, K. Leong, O.K. Farha, M. Allendorf, R.P. Van Duyne, J.T. Hupp, Metal-organic framework materials as chemical sensors, Chem. Rev. 112 (2012) 1105–1125.
[13] S. Hermes, F. Schröder, R. Chelmowski, C. Wöll, R.A. Fischer, Selective nucleation and growth of metal – organic open framework thin films on patterned COOH/$CF_3$-terminated self-assembled monolayers on au(111), J. Am. Chem. Soc. 127 (2005) 13744–13745.
[14] E. Biemmi, C. Scherb, T. Bein, Oriented growth of the metal organic framework

$Cu_3(BTC)_2(H_2O)_3{\cdot}xH_2O$ tunable with functionalized self-assembled monolayers, J. Am. Chem. Soc. 129 (2007) 8054–8055.
[15] O. Shekhah, H. Wang, S. Kowarik, F. Schreiber, M. Paulus, M. Tolan, C. Sternemann, F. Evers, D. Zacher, R.A. Fischer, C. Wöll, Step-by-step route for the synthesis of metal-organic frameworks, J. Am. Chem. Soc. 129 (2007) 15118–15119.
[16] G. Lu, J.T. Hupp, Metal-organic frameworks as sensors: a ZIF8 based Fabry-Pérot device as a selective sensor for chemical vapors and gases, J. Am. Chem. Soc. 132 (2010) 7832–7833.
[17] P. Falcaro, R. Ricco, C.M. Doherty, K. Liang, A.J. Hill, M.J. Styles, MOF positioning technology and device fabrication, Chem. Soc. Rev. 43 (2014) 4413–4461.
[18] O. Shekkhah, J. Liu, R.A. Fischer, Ch. Wöll, MOF thin films: existing and future applications, Chem. Soc. Rev. 40 (2011) 1081–1106.
[19] B. Paschke, A. Wixforth, D. Denysenko, D. Volkmer, Fast surface acoustic wave-based sensors to investigate the kinetics of gas uptake in ultra-microporous frameworks, ACS Sens 2 (2017) 740–747.
[20] M.D. Allendorf, R.J.T. Houk, L. Andruszkiewicz, A.A. Talin, J. Pikarsky, A. Choudhury, K.A. Gall, P.J. Hesketh, Stress-induced chemical detection using flexible metal-organic frameworks, J. Am. Chem. Soc. 130 (2008) 14404–14405.
[21] C. Scherb, A. Schödel, T. Bein, Directing the structure of metal–organic frameworks by oriented surface growth on an organic monolayer, Angew. Chem. 120 (2008) (5861 – 5683).
[22] O. Shekkhah, H. Wang, D. Zacher, R.A. Fischer, C. Wöll, Growth mechanism of metal-organic frameworks: insights into the nucleation by employing a step-by-step route, Angew. Chem. Int. Ed. 48 (2009) 5038–5041.
[23] D. Zacher, R. Schmid, C. Wöll, R.A. Fischer, Surface chemistry of metal–organic frameworks at the liquid–solid Interface, Angew. Chem. Int. Ed. 50 (2011) 176–199.
[24] L.E. Kreno, J.T. Hupp, R.P. Van Duyne, Metal-organic framework thin film for enhanced localized surface Plasmon resonance gas sensing, Anal. Chem. 82 (2010) 8042–8046.
[25] R.C. Arbulu, Y.-B. Jiang, E.J. Peterson, Y. QinHou, Metal–Organic Framework (MOF) Nanorods, Nanotubes, and Nanowires, Angew. Chem Int. Ed. 130 (2018) 5915–5919.
[26] C. Hou, Q. Xu, J. Peng, Z. Ji, X. Hu, (110)-oriented ZIF-8 thin films on ITO with controllable thickness, Chem. Phys. Chem. 14 (2013) 140–144.
[27] H. Bux, A. Feldhoff, J. Cravillon, M. Wiebcke, Y.-S. Li, J. Caro, Oriented zeolitic imidazolate framework-8 membrane with sharp $H_2/C_3H_8$ molecular sieve separation, Chem. Mater. 23 (2011) 2262–2269.
[28] C. Dimitrakakis, C.D. Easton, B.W. Muir, B.P. Ladewig, M.R. Hill, Spatial control of Zeolitic Imidazolate framework growth on flexible substrates, Cryst. Growth Des. 13 (2013) 4411–4418.
[29] R. Ameloot, L. Stappers, J. Fransaer, L. Alaerts, B.F. Sels, D.E. De Vos, Patterned growth of metal-organic framework coatings by electrochemical synthesis, Chem. Mater. 21 (2009) 2580–2582.
[30] S. Eslava, L. Zhang, S. Esconjauregui, J. Yang, K. Vanstreels, M.R. Baklanov, E. Saiz, Metal-organic framework ZIF8 films as low-k dieelectrics in microelectronics, Chem. Mater. 25 (2013) 27–33.
[31] E. Delamarche, B. Michel, H. Kang, C. Gerber, Thermal stability of self-assembled monlayers, Langmuir 10 (1994) 4103–4108.
[32] D. Käfer, G. Witte, P. Cyganik, A. Terfort, C. Wöll, A comprehensive study of self-assembled monolayers of anthracenethiol on gold: solvent effects, structure, and stability, J. Am. Chem. Soc. 128 (2006) 1723–1732.
[33] A. Schaller, A. Ullrich, S. Horn, D. Volkmer, Selective growth of MFU-4l single crystals on microstructured plasma polymer coatings, Chem. Comm. 51 (2015) 12494–12496.
[34] A. Steinbach, A. Tautzenberger, A. Schaller, A. Kalytta-Mewes, S. Tränkle, A. Ignatius, D. Volkmer, Plasma-enhanced chemical vapor deposition of n-heptane and methyl methacrylate for potential cell alignment applications, Appl. Mater. Interfaces 4 (2012) (5196–5023).
[35] S. A. Letsche, Polymerdünnfilme als Template für die Darstellung anorganischer Nanopartikel, PhD Thesis, University of Ulm, 2012.
[36] S. Biswas, M. Grzywa, H.P. Nayek, S. Dehnen, I. Senkovska, S. Kaskel, D. Volkmer, A cubic coordination framework constructed from benzobistriazolate ligands and zinc ions having selective gas sorption properties, Dalton Trans. 33 (2009) 6487–6495.